https://doi.org/10.5194/nhess-2022-126
Preprint. Discussion started: 27 April 2022

Natural Hazards and Earth System Sciences
Discussions
Open Access
EGU

Characteristics of consecutive tsunamis and resulting tsunami behaviors in southern Taiwan induced by the doublet earthquakes on 26 December 2006

An-Chi Cheng[1,2], Anawat Suppasri[2,3], Kwanchai Pakoksung[3], Fumihiko Imamura[2,3]

[1]Civil and Environmental Engineering, Graduate School of Engineering, Tohoku University, 6-6-06 Aoba, Aramaki-Aza, Aoba, Sendai 980-0845, Japan

[2]WISE Program for sustainability in the Dynamic Earth, Tohoku University, 6-3 Aoba, Aramaki Aza, Aoba, Sendai 980-8578, Japan

[3]International Research Institute of Disaster Science, Tohoku University, 468-1 Aoba, Aramaki-Aza, Aoba, Sendai 980-0845, Japan

Correspondence to: An-Chi Cheng (cheng.anchi.r6@dc.tohoku.ac.jp)

Abstract. Consecutive M_w 7.0 and M_w 6.9 submarine earthquakes occurred offshore Hengchun Peninsula, Taiwan on 26 December 2006. A small tsunami was generated, and recorded at tide gauge stations for the first time. This important event attracted public interest as it was generated by doublet sources and demonstrated tsunami risk in Taiwan. This study analyzed tide gauge tsunami waveforms and numerical simulations to understand the source characteristics and resulting tsunami behaviors. The maximum wave heights at three stations were 0.08 m (Kaohsiung), 0.12 m (Dongkung), and 0.3 m (Houbihu), and only Houbihu recorded the first wave crest as the largest. The tsunami durations were 3.9 h at Dongkung, and more than 6 h at Kaohsiung and Houbihu. Spectral analyses detected dominant periodic components of spectral peaks on tsunami waveforms. The period band from 15.5-26.6 min was identified as the tsunami source spectrum, and the approximate source area for the consecutive tsunamis was constrained to be 800 km^2. Comparing the simulated tsunami waveforms to observed tsunami waveforms showed that the GCMT focal mechanisms explained the observations at all three stations better than the USGS solutions. Numerical simulations based on real and hypothetical bathymetry examined its influence on the transmission of tsunami waves. The results revealed that wave trapping was connected to wave refraction caused by bathymetry. Trapped waves interfered with incident waves at shelf edges amplified tsunami waves and prolonged oscillations, which explained unusual observations recorded by the tide gauges. These elucidate the generation of the consecutive 2006 tsunamis, and consequent tsunami behaviors in southern Taiwan, contributing essential knowledge for tsunami warning and coastal emergency response in Taiwan to reduce disaster risk.

https://doi.org/10.5194/nhess-2022-126
Preprint. Discussion started: 27 April 2022

Natural Hazards and Earth System Sciences
Discussions

1. Introduction

Taiwan is located at the plate margins of the Eurasian plate and the Philippine Sea plate from the southeast. The abrupt movement of plates results in active seismic activity at the boundary area, such as Manila Trench and Ryukyu Trench. The Manila Trench and Ryukyu Trench are located offshore Taiwan, and have been identified as hazardous tsunamigenic regions, as both have the potential to generate megathrust earthquakes and causes severe tsunami impacts on coast plains (Liu et al., 2009; Megawati et al., 2009; Wu and Huang, 2009; Li et al., 2016; Sun et al., 2018; Qiu et al., 2019). In addition to potential megathrust earthquakes, the historical earthquake tsunamis in Taiwan are well recorded in ancient and written documents. Examples include the 1781/1782 Jiateng harbor flooding and tsunami event (Okal et al., 2011; Li et al., 2015), and the 1867 northern Taiwan earthquake (Cheng et al., 2016; Sugawara et al., 2019).

Two large earthquakes occurred off the coast of Hengchun Peninsula, Taiwan on 26 December 2006. The first earthquake occurred at 12:26:21 UTC (i.e., 20:26:21 Taiwan Standard Time), and was followed by second earthquake 8 min later at 12:34:15 UTC (i.e., 20:34:15 Taiwan Standard Time). The Central Weather Bureau (CWB) catalog (R.O.C.) located the epicenter of the first shock at 21.67° N and 121.56° E, and the second shock at 21.97° N and 121.42° E. According to the USGS earthquake catalog, the respective magnitudes of these two earthquakes were suggested to be M_w7.0 for the former, and M_w 6.9 for the latter. Sharing similar magnitudes, and very close epicenters, these two successive earthquakes are considered as doublet earthquakes event (Lay and Kanamori, 1980). The 2006 earthquakes in southern Taiwan were regarded as the largest event in the past hundred years (Wu et al., 2009). Several casualties and some structural damages were reported in southern Taiwan during this seismic event (National Disaster prevention and Protection Commission, R.O.C., 2007). The locations of Hengchun Peninsula and the epicenters of the successive earthquakes are shown in Figure 1.

A small tsunami was generated after the successive strong motions of these earthquakes. The tsunami propagated toward, and reached the western coast of southern Taiwan immediately after the earthquakes. Although no coastal run-up or inundation was reported, the tsunami signals were instrumentally recorded at CWB tide gauge stations in southern Taiwan for the first time. The December 2006 tsunami was an important event and attracted public interest, as it was a rare tsunami event generated by successive earthquakes, and was a new issue among social communities and ordinary persons in Taiwan about tsunamis. This recent tsunami not only corroborates the tsunami risk in Taiwan, but also heightens the awareness of disaster risk management, such as preparedness, and mitigation countermeasures for the next tsunamis.

Following the December 2006 earthquake tsunami, some anomalous observations were reported from the CWB tide gauges along the southern coast of Taiwan. First, the initial wave crest was not recorded as highest. It has been a common understanding that the maximum wave should coincide with the first wave in the event of a near-field tsunami. However, some stations did not show the first wave crest as the largest during the December 2006 tsunami. Such an amplified tsunami was contradictory to the ordinary sense of

https://doi.org/10.5194/nhess-2022-126
Preprint. Discussion started: 27 April 2022


Natural Hazards and Earth System Sciences
Discussions

near-field tsunamis, but important as it might followed by a higher wave and could consequently upgrade the issued warning level (Suppasri et al., 2017; Suppasri et al., 2021). Second, prolonged durations of the tsunami were recorded at some coastal sites. The long tsunami oscillation occurred because of the transport of high energy waves along the coast without decay. The above recorded evidence from tide gauges indicates that different tsunami behaviors might have been presented in southern Taiwan during the 2006 tsunami. This warranted a detailed investigation to clarify the unknown features of these complicated tsunami waveforms which might cause unexpected cascading coastal impacts from tsunamis.

In addition to the unusual tsunami observations, another issue was which tsunami source model could better explain the successive tsunamis given the available observations at tide gauge stations. Wu et al., 2008, deterministically selected the Global Centroid Moment Tensor (GCMT) model of fault source geometries, and applied empirical scaling relations to reconstruct earthquake tsunami scenarios. Nevertheless, this important issue remains to be clarified and difficult to be constrained because of insufficient seismic data and the inconsistent faulting properties from Moment Tensor solved by various agencies. To overcome this, examining earthquake tsunami scenarios and tsunami generation by comparing observation records from tide gauge stations is critical.

Based on the above background, the primary intent of this article is to address all aforementioned questions and issues related to the 2006 tsunami, and to provide some results. The content of this article was organized as follows. First, the observed tsunami waveforms are presented to determine the physical characteristics of the tsunami, and employed as inputs for root mean square (RMS) analyses to detect the tsunami duration. Second, the spectral analyses are performed to detect the periodic components of tsunami waves subject to identification of the tsunami source spectrum and shelf oscillation mode. Then, numerical simulations are conducted to validate the designed earthquake tsunami scenario, and to justify the tsunami behaviors around southern Taiwan. The December 2006 earthquake tsunami represents a unique and recent incident in Taiwan; therefore, the reconstruction and findings could not only help to further understand the tsunami generation and important behaviors responsible for the tsunami hazards to the island of Taiwan, but also have implications for tsunami warning and disaster risk management.

2. Data and methods

2.1 Tide gauge tsunami data

In general, the time history data of sea levels recorded at coastal sites provide one possible method to study tsunami patterns. To investigate the tsunami characteristics of the 2006 tsunami, the sea level records from tide gauge stations were employed for analysis in the present study. For this purpose, the recorded data from three tide gauge stations (Kaohsiung, Dongkung, and Houbihu) located in southern Taiwan were obtained. These tide gauge stations are operated and maintained by the CWB, R.O.C. All stations recorded sea levels with a sampling rate of 6 min. In this doublet event, the first and second earthquakes occurred at 20:26:21 and 20:34:15 (Taiwan standard time), respectively. Hence, the tide gauge records for 28 h (from

https://doi.org/10.5194/nhess-2022-126
Preprint. Discussion started: 27 April 2022


Natural Hazards and Earth System Sciences
Discussions

8:00 26 December 2006 to 12:00 27 December 2006, Taiwan standard time) were adopted for analysis. To approximate the wave components of the tsunami and to remove the low-frequency noise that was attributed to the tidal effect, the sea level records in tide gauge stations were de-tided by removing the long period (> 2 h) tidal constituents. The original data recorded at tide gauge stations in southern Taiwan are shown in Figure 2a, and the de-tided data are presented in Figure 2b. The locations of the tide gauge stations are shown in Figure 3.

The tsunami durations represent the duration time of high-energy tsunami waves persisting in a coastal site of observation. The tsunami duration at all stations was identified based on the calculation of RMS sea levels, indicating the elapsed time of the wave amplitude above the level of normal oscillation before the tsunami wave arrived (Heidarzadeh, 2021). The RMS analysis calculated the moving average of the recorded sea level along moving time window of 24 min. The equation for calculating RMS sea level is given as:

$$S(t) = \sqrt{\frac{1}{w}\int_{t-\frac{w}{2}}^{t+\frac{w}{2}} h(x)^2 \, dx} \quad (1)$$

In this equation, S (t) represents the RMS sea level at time step t, h (t) denotes the recorded sea level at time t, and w stands for the moving time window. In the present study, the length of tsunami data employed for RMS analysis is 12 h, which includes 120 data points, ranging from 17:00 on 26 December 2006 to 5:00 27 on December 2006 (Taiwan standard time). A similar method has been applied in the study of Hayashi et al., 2012.

2.2 Spectral analyses

To apply spectral analyses to tsunami data, two types of analyses were included and processed in this study: Fourier analysis and wavelet (time-frequency) analysis. Fourier analysis is based on the fast Fourier transform (FFT) algorithm, applied based on the updated open-source library Numpy in the Python package (Harris et al., 2020). Fourier analysis was performed to estimate the spectral components of the time history data of the tsunami waveform. The total data points of the tsunami waveform inputted for Fourier analysis covered 540 min, which included 90 data points ranging from 3 h before to 6 h after the tsunami, as the sampling rate of the data was 6 min. The Fourier analysis was applied to background (i.e., -3-0 h data) and tsunami signals (i.e., 0-3 h and 3-6 h), separately, to identify significant changes in spectral energy associated with the tsunami. Additionally, the spectral ratio was computed for tsunami spectra to exclude the local modes of coastal sites from periodic components. Wavelet analysis was computed based on the Morlet mother function, as suggested by Torrence and Compo, 1988. Wavelet analysis detects the periodic change in spectral peaks over time history. The length of tsunami data input in wavelet analysis was 15 h (15:00 on 26 December 2006 to 06:00 on 27 December 2006, Taiwan standard time). A similar method has

https://doi.org/10.5194/nhess-2022-126
Preprint. Discussion started: 27 April 2022

been widely applied to solve frequency-time problems for many recent tsunami events, such as the 2018 Sulawesi tsunami, Indonesia, and the 2020 Aegean Sea earthquake tsunami (Heidarzadeh, 2019; Heidarzadeh, 2021).

2.3 Numerical tsunami simulation

Numerical simulation is a common method that promotes understanding of tsunami characteristics and coastal impacts by reproducing historical tsunamis. Examples comprise the 2004 Indian Ocean earthquake tsunami, and the 2011 Tohoku-Oki earthquake tsunami (Suppasri et al., 2012; Suppasri et al., 2014). In this study, the Tohoku University's Numerical Analysis Model for Investigation of Near-field tsunamis, No. 2 (TUNAMI-N2) was employed to perform tsunami propagation. This model was mainly developed to investigate near-field tsunamis based on nonlinear shallow water equations in the numerical domain adopting a Cartesian coordinate (Imamura, 1995). In the TUNAMI-N2 model, the nonlinear theory of shallow water equations was solved by the leap-frog scheme to model tsunami propagation from source to nearshore region and the finite difference methodology was applied to solve the nonlinear equations. In the governing equations, bottom friction term was represented by the Manning roughness coefficient, which was set equal to 0.025 s $m^{-1/3}$, assuming the seafloor of the model domain had a perfect condition (Kotani, 1998). To ensure the run stability, the numerical system was solved every 0.1 s for each time step to satisfy the Courant-Friedrichs-Lewy (CFL) condition. The total computational time was 300 min for all tsunami simulations conducted in this study.

2.4 Earthquake tsunami scenarios

The December 2006 tsunami event was triggered by successive earthquakes of M_w7.0 and M_w 6.9 that occurred offshore the Hengchun Peninsula. It is necessary to consider both earthquakes as a doublet source for the generation mechanism of the tsunami. Doublet earthquakes have been investigated by many seismological agencies, including the CWB, USGS and GCMT. Several moment tensor solutions have been proposed to explain the focal mechanisms of the two earthquakes. Each moment tensor solution comprises two nodal planes, which suggests two possibilities of faulting for each earthquake. The earthquake faulting characteristics of the two successive earthquakes, determined by the GCMT and USGS, were presented as beach balls in Figure 3.

In this study, two earthquake tsunami scenarios were constructed to examine the generation mechanism of these doublet tsunamis, accounting for the NP1 fault planes from each earthquake introduced by the GCMT and USGS. The first earthquake tsunami scenario was based on the GCMT moment tensor solution, with a strike of 165°, dip of 30°, rake of -76°, and depth of 19.6 km for the first earthquake, and a strike of 151°, dip of 48°, rake of 0°, and depth of 32.8 km for the second earthquake. Another scenario applied by the USGS solution, with a strike of 171°, dip of 24°, rake of -61°, and depth of 25.5 km for the first earthquake, and a strike of 151°, dip of 48°, rake of 0°, and depth of 32.8 km for the second earthquake.

https://doi.org/10.5194/nhess-2022-126
Preprint. Discussion started: 27 April 2022


Natural Hazards and Earth System Sciences
Discussions

175 The parameters of earthquake focal mechanisms are summarized in Table 1.

In addition to the fault parameters of the earthquake rupture mechanisms, the rupture dimensions and slip amount of earthquake faults are essential information. The fault rupture dimensions of the two earthquakes were estimated based on the inverse method of the tsunami source spectrum given by the spectral analyses. The fault length was approximately 40 km, and the fault width was 20 km, for the two
180 earthquakes, as detailed in Section 3.1. The respective values of the uniform slip parameter were estimated using Papazachos et al.'s, (2004) empirical scaling relations, where 1.18 m was estimated to the first earthquake, and 0.9 m for the second earthquake.

For tsunami generation, the initial sea surface elevation was calculated using the theory of Okada, 1985 based on final determined fault parameters for the two earthquake tsunami scenarios, GCMT and USGS.
185 In the theory of Okada, 1985, an elastic deformation of sea surface elevation based on rectangular fault rupture was assumed for tsunami generation. Here, the horizontal effect of Tanioka and Satake, 1996, was also considered for tsunami generation because of the strike-slip nature of the second earthquake, and the complex characterize of the bathymetry offshore. Although Li, 2015 suggested possible submarine landslide sources in this region, the coupled source of submarine landslides was excluded from the scope
190 of tsunami generation for this event because of the small tsunami, which could not have been caused submarine landslides. Noted here that the initial sea surface elevation of the second tsunami overlapped with the calculated surface elevation at elapsed time of 8 min for the overall generation of this tsunami event according to the original earthquake time. The initial sea surface elevations of the earthquake tsunami scenarios are shown in Figure 4.

195 To examine whether the GCMT scenario or the USGS scenario could better represent the December 2006 tsunami, simulated tsunami waveforms were compared to observations at all three stations in southern Taiwan. The earthquake tsunami scenario that could produce tsunami waveforms consistent with the observations was chosen to represent the tsunami generation for numerical simulation in the next section.

200 **2.5 Effect of bathymetry on tsunami propagation based on actual and hypothetical bathymetry**

To examine any significant change in tsunami wave transmission around southern Taiwan that could be recognized due to the bathymetry effect during the passage of the 2006 tsunami, the experiment was performed based on numerical tsunami simulation applying two bathymetric scenarios to the region of interest: actual and hypothetical bathymetry. The actual bathymetry was created based on the original
205 bathymetric grid obtained from GEBCO, 2021 with a 15 arc-second resolution, and then resampling to 450 m grids (Figure 3).

For the hypothetical scenario, the bathymetric grid was constructed by eliminating the shallow bathymetry configuration (i.e., for sea depths shallower than 500 m) with a constant and flattened sea bottom at a depth of 500 m from the original bathymetric grid. Notably, the 500 m depth contour was
210 defined as indicative because the bathymetric gradient of coastal water for depths shallower than 500 m in

https://doi.org/10.5194/nhess-2022-126
Preprint. Discussion started: 27 April 2022


Natural Hazards and Earth System Sciences
Discussions

front of southern Taiwan is very gentle, and therefore identified as the continental shelf. The comparison designed here was intended to evaluate how tsunami wave directivity could be changed due to the bathymetric effect, and to examine whether such a factor played an important role in wave trapping over continental shelves in front of southern Taiwan during the passage of the 2006 tsunami.

3 Analyses of tsunami waveforms and tsunami durations

3.1 Physical characteristics of tsunami waveforms

The December 2006 earthquake tsunami was observed at several tide gauges at coastal sites located along the southwestern coast of Taiwan. The tsunami observations are plotted in Figure 5a. The initial wave arrived at all three tide stations in southern Taiwan with an amplitude sign of a trough wave. The travel times of the initial wave to all stations were recorded: 16 min to Houbihu, 28 min to Dongkung, and 52 min to Kaohsiung. The initial wave was recorded as -0.12 m in Houbihu, -0.09 m in Dongkung, and 0.06 m in Kaohsiung, respectively. Following the trough sign of the initial wave, the first wave crest record at Houbihu was 0.3 m, which was approximately 3 times greater than that at Dongkung, and 4 times larger than that at Kaohsiung. This was natural because Houbihu was the station closest to the epicentral region, and therefore had a shorter arrival time and was relatively sensitive to the surface elevation change in sea level induced by the tsunami. The maximum wave heights were recorded as 0.08 m (Kaohsiung), 0.12 m (Dongkung), and 0.3 m (Houbihu). In Kaohsiung and Dongkung, the maximum height was not recorded for the initial wave. The maximum wave height appeared 36 min after the initial wave arrived at Kaohsiung, and after 24 min at Dongkung, indicating a pattern of wave amplification at these stations. These results suggest that a different mechanism of tsunami waves was active at these coastal sites during the passage of the 2006 tsunami. The locations and details of tide gauge observations are summarized in Table 2a, for wave amplitude, and Table 2b for arrival time and visible period.

In addition to significant differences in wave amplitude and arrival time, the tsunami records at each station also varied in terms of visible wave periods. The visible period of the tsunami wave at Kaohsiung was recorded from 30-48 min based on the tsunami waveform, which was approximately two times longer than those observed at Dongkung and Houbihu from 18-24 min. This indicated that the wave components with shorter periods were not well recorded in Kaohsiung with coarse sampling rate of 6 min. Therefore, the actual maximum wave height of the tsunami waveform recorded in Kaohsiung might have been higher than that presented in this article (Figure 5a).

3.2 Tsunami durations

Another issue was to determine the tsunami duration at each station because it can help to identify the length of wave oscillation at a coastal site due to the tsunami. Typically, tsunami duration describes the elapsed time during which a high-energy wave at a tide gauge station exceeds the mean sea level of normal oscillation. The normal oscillation was defined as the site-specific oscillation at each station before the

https://doi.org/10.5194/nhess-2022-126
Preprint. Discussion started: 27 April 2022


Natural Hazards and Earth System Sciences
Discussions

tsunami arrived. The RMS analysis was applied to the recorded sea level data at each station. The results of the RMS analysis are plotted in diagrams, as shown in Figure 5b.

The RMS sea level diagram illustrates how long the high energy wave persisted at each station. Accordingly, the tsunami duration was determined through the comparison of RMS sea level and basic oscillation in sea level at each station. The maximum RMS sea level derived at Houbihu station was estimated to be 2-3 times higher than those at Dongkung and Kaohsiung stations. The calculated tsunami duration at Dongkung was as much as 3.9 h, while the tsunami continued for more than 6 h in Kaohsiung and Houbihu. The abnormally long tsunami in Kaohsiung and Houbihu suggested that a pattern of long-lasting oscillation might have occurred along the western coast during the 2006 tsunami.

Generally, several oscillation modes are expected to be induced during a tsunami event associated with the tsunami source, propagation path, and topographic effects (Rabinovich, 1997; Rabinovich et al., 2013). An island setting such as Taiwan, where insular shelves and gentle slopes exist, commonly traps waves over the continental shelf during the passage of tsunamis (Roeber et al., 2009). The trapped wave propagates along the coastline, and normally triggers various oscillation modes in coastal water due to the interference of wave reflection at the edge of continental shelves (Yamazaki et al., 2011). The wave resonance of these oscillation modes with the fundamental modes of the continental shelf can enhance coastal hazards with amplified amplitudes and long tsunami durations (Wang et al., 2020). The triggered oscillation modes are expected to be mixed with the tsunami source spectrum in the observation records from coastal sites. To identify these modes from the tsunami source spectrum, spectral analyses were performed on the observation records at all three tide gauge stations in southern Taiwan, as detailed in next section.

4 Spectral analysis

4.1 Tsunami source spectra

To examine the spectral characteristics of tsunami waves, Fourier analysis was applied to tsunami data recorded at all tide gauge stations in southern Taiwan. In the analysis, the background spectra were calculated in addition to the tsunami spectra to compare tsunami effect with the background signals. Here, the background spectra were defined as components of the spectra recorded at each station before the tsunami arrival. Figure 6a shows the results of the tsunami and background spectra for each station. A visible gap appears in the spectral energy between the tsunami and background spectra at all stations, indicating the energy transmitted by the tsunami. The dominant periodic values of spectral peaks for background and tsunami signals are listed in Table 3a.

Clearly, the peaks of tsunami spectra were estimated to be different from background spectra at all stations. The spectral peaks of background spectra were found to vary by station, which revealed that the local modes should vary according to the coastal sites. In theory, as suggested by Toguchi et al., 2018, the local modes are dependent on the topographic influence on background conditions. To identify the spectral components from the tsunami, the independent site-specific local modes were obtained by calculating

https://doi.org/10.5194/nhess-2022-126
Preprint. Discussion started: 27 April 2022


Natural Hazards and Earth System Sciences
Discussions

record spectra as a ratio of background spectra. The spectral ratio is defined by the equation shown below:

$$S_{tsunami}(\omega) = \frac{S_{record}(\omega)}{S_{background}(\omega)} \quad (2)$$

In this equation, S_{record} (ω) presents the spectral components recorded at the tide gauge station, $S_{background}$ (ω) denotes the background spectra, and $S_{tsunami}$ (ω) represents tsunami spectra. Here, note that this equation assumes equivalent background spectra before and after the arrival of tsunami waves, indicating that there was no large change in coastal topography during the tsunami event. Although many earlier studies had reported that coastal topography might be largely changed during a massive tsunami event (e.g., Sugawara, 2018; Masaya et al., 2020), this was not the case for the 2006 tsunami because the wave was small. Therefore, the dominant peaks of the spectral ratios were connected to either the tsunami source or perhaps a pattern of non-source oscillation.

In theory, according to Rabinvoich, 1997, tsunami source periods are those periodic components that primarily appear in coastal observations close to the epicenters, and the first train of tsunami waves is usually contributed by the tsunami source. Accordingly, the tsunami source periods were estimated from the dominant periods of the first wave train signals given by the Fourier analyses. To determine the tsunami source periods, the recorded observations of 6 h signals at all stations were first separated into two temporal segments of 0-3 h and 3-6 h, and both values were then employed as inputs for spectral estimation. The tsunami source periods were determined by comparing the dominant spectral peaks that appeared in the signals of the former temporal segment (i.e., 0-3 h after the earthquake) at all stations. Figure 6b shows the spectral ratios for tsunami spectra at all stations, and the corresponding periods of spectral ratio peaks are listed in Table 3b.

The Houbihu station is the closest observation site to the epicentral region. Among the dominant periods at Houbihu station, the period band of 15.5-26.6 min most likely presented the source periods of the 2006 Hengchun tsunami since the dominant periods within this band mainly appeared at Houbihu station, and were mostly visible at other sites in the signals of early temporal segments. Other peak periods such as 31.0 min, 46.5 min and 62 min, disappeared at some stations.

Next, based on the tsunami source periods determined from Fourier analyses, the fault dimensions of the tsunami source can be estimated. In general, an earthquake with a larger size can ordinarily generates a larger tsunami wave with a longer period. For instance, the major periods of the 2011 Tohoku-Oki earthquake tsunami was reported to be 37-67 min associated with the magnitude M_w 9.0 earthquake (Heidarzadeh and Satake, 2013), while shorter dominant periods of 10-22 min were found for the 2013 Santa Cruz tsunami, a M_w 8.0 earthquake (Heidarzadeh, 2016). According to the theory, as introduced by Rabinovich, 1997, the approximate dimensions of fault rupture can be estimated using the empirical formula as defined below:

https://doi.org/10.5194/nhess-2022-126
Preprint. Discussion started: 27 April 2022

$$L = \frac{T_n}{2} n\sqrt{gh}; \quad n = 1,2,\ldots \tag{3}$$

where g stands for the gravitational acceleration and is set to a constant value of 9.81 m s^{-2}, h presents the seafloor depth around the tsunami source region, L denotes rupture dimensions of length or width, and T is the dominant periodic component dictated by the tsunami source. The approximate source region could be illustrated based on the aftershock distribution one day after the first earthquake occurred. The depth of the seafloor around the tsunami source region was approximately 50-550 m (Figure 3), and a mean seafloor depth of 300 m could be calculated. Considering tsunami source periods of 15.5, 20.7, and 26.6 min, and seafloor depths of ~600 m, the results given by equation (3) are plotted in Figure 7. From the results, lengths of 20-40 km most likely represented the fault dimensions for the two successive earthquakes in this doublet event. The longer rupture dimension of 40 km was considered the fault length, and 20 km was considered the fault width. The approximate source area of these two earthquakes was estimated to be 800 km^2. These values were fairly consistent with the approximate fault areas of 794 km^2, associated with a M_w 7.0 normal fault earthquake, and 738 km^2 associated with a M_w 6.9 strike-slip fault according to the empirical scaling relations of Papazachos et al., 2004. Based on these results, the tsunami sources were determined to 40 km × 20 km for the two earthquakes, and the periodic components of 15.5-26.6 min could be interpreted as the tsunami source spectrum. Other dominant peaks of the spectral ratio might be connected to the modes of tsunami-induced shelf resonance.

4.2 Tsunami-induced shelf resonance modes

In addition to the Fourier analyses, wavelet (time-frequency) analyses were also applied to 15 h of tsunami data (i.e., 15:00 26 December 2006 to 6:00 27 December 2006, Taiwan standard time) at CWB tide gauge stations in southern Taiwan. Wavelet analyses are commonly employed as a method to examine periodic variations over time series through the distribution of tsunami spectral energy. Figure 8. shows the tsunami wavelets derived from tsunami records observed at each station. According to the wavelet plots at all stations, period bands of 15.5-26.6 min are clearly recorded in the first wave train signals at all stations, indicating that periodic components of 15.5-26.6 min were dictated by the tsunami source during the 2006 Hengchun tsunami. At Kaohsiung, the tsunami energy became apparent with periods of 16 min and 36 min approximately 3 h after the first tsunami arrival at this station. In the period channel of 16 min, the oscillation was preserved for approximately 5 h, while the 36 min channel was occupied by a high-energy wave for more than 9 h. At Houbihu, more energy was channeled in the periods band of 15.5-26.6 min than at other stations soon after the first earthquake. This was reasonable because Houbihu was the station closest to the epicentral region, and therefore considered to be more sensitive to the tsunami source than the others. Following the first wave train, the next phase produced a significantly persistent long-lasting oscillation (i.e., for more than 4 h) in the period channels of 16 min, 16.4 min, 20 min, 22.5 min, 25.7 min, 30 min, 36

https://doi.org/10.5194/nhess-2022-126
Preprint. Discussion started: 27 April 2022

min, and 60 min. These wave energy channels commenced their oscillation approximately 2 h after the first earthquake. These periodic components were considered possible contributors to long tsunami oscillations because these periods were dominant for prolonged times, and the wave resonance of the tsunami wave and fundamental oscillation modes of the continental shelf commonly require for some time to be formed. Among these periods, the periodic component of 36 min was most likely the mode of shelf oscillation since it was not included in the source period band of 15.5-26.6 min and was visible at only Kaohsiung and Houbihu station, where long tsunami durations of more than 6 h were recorded (Figure 5). Hence, as revealed from the wavelet plots of later wave train signals, the abnormally long tsunami duration times recorded at Kaohsiung and Houbihu stations might be attributed to wave resonance over the continental shelves of southern Taiwan during the passage of the 2006 tsunami.

5 Numerical tsunami simulations

5.1 Validity of earthquake tsunami scenarios and numerical results

In addition to the analysis on tsunami waveforms, numerical simulation was performed to investigate the characteristics of the triggered doublet earthquake tsunami in southern Taiwan. For this purpose, the earthquake tsunami scenario for tsunami generation of the December 2006 tsunami had to be identified. Here, two different patterns of the earthquake tsunami scenario were examined as possible generation mechanisms of the 2006 tsunami. One possible scenario was constructed using focal mechanisms solved by the GCMT. The other scenario was dependent on the earthquake rupture pattern from the USGS solution.

To examine the earthquake tsunami scenarios for the December 2006 tsunami and the validity of the numerical results, the tsunami waveforms were simulated using the GCMT and USGS scenarios, and compared to the observations recorded at three tide gauge stations around southern Taiwan. Noted here that the present study could validate the numerical results based on tsunami waveforms at each station only at a 6 min rate because there were no runup or inundation recordings during the 2006 tsunami. Figure 9 presents a comparison of the simulated and observed tsunami waveforms at all stations for the two tsunami scenarios. The details of the simulated and observed tsunami waveforms at each station are listed in Table 4a, including the wave amplitudes and Table 4b gives the arrival times.

From the comparison of simulated and observed tsunami waveforms (Figure 9), either the GCMT or USGS scenario could produce first and second cycles of tsunami waveforms that were reasonably consistent with observations at Dongkung and Houbihu stations, but significantly discrepant at Kaohsiung station. This could be attributed to the coarse sampling rate of tide gauge data, where the tsunami waveform was not clearly recorded, as described in Section 3.1. Nevertheless, the GCMT scenario showed simulated values generally closer to the observations than USGS scenario. This indicated that the GCMT scenario, rather than the USGS scenario, had better reproductivity for tsunami waveforms at tide gauge stations. Hence, the GCMT scenario was considered a favorable model for representing tsunami generation of the 2006 southern Taiwan tsunami for numerical simulation in this article.

https://doi.org/10.5194/nhess-2022-126
Preprint. Discussion started: 27 April 2022

5.2 Effect of bathymetry to tsunami propagation in southern Taiwan

It is commonly understood that tsunami travel with velocity that is mainly governed by seafloor depths. A tsunami propagates at a slower speed when the tsunami wave enters the shallow water from deeper water. The significant change in propagation speed allows the tsunami to change its wave direction. The propagation simulation results of the actual bathymetry scenario are illustrated by snapshots, as shown in Figure 10. Figure 10 presents the wave reflection and refraction, and shows how tsunami waves repeatedly changed their directions among the continental shelves around southern Taiwan after tsunami wave arrived.

An inspection of Figure 10 indicates a trough sign for the tsunami wave along the coastline immediately after the first tsunami generation (Figure 10a), which was followed by the second tsunami at 8 min later. The initial wave crest reached the southern part of Hengchun Peninsula after 8 min (Figure 10b). The bathymetry in the front had shallow depths (e.g., water depths less than 500 m) compared to the open ocean. According to this bathymetric feature, the tsunami wave was significantly amplified due to wave shoaling and refracted toward the northern part of the epicentral region, and then concentrated into the embayment of the western coast. Only rare tsunamis were reflected back to the open ocean or transmitted to the eastern coast (Figure 10c). In the tsunami source region, the water depth gradually increased toward the southwest. The bathymetry in front of eastern coast was deeper and had a steep slope. These features enabled the tsunami wave to change its original path to the north, and focus inside the embayment after 18 min. After arriving at the western coast, the tsunami wave was reflected after 28 min (Figure 10d). The reflected wave from the coast tended to be radiated offshore. However, it was not fully radiated offshore, instead, was again reflected at the boundary of the shelf, and refracted toward the coast. According to the process of multiple wave reflections, the tsunami wave was transmitted north as far as the Dongkung and Kaohsiung stations, indicating that the tsunami wave was trapped over the shelves during its passage. Due to this fluctuation, the high-energy tsunami wave remained along the western coast for a long time, which could be clearly seen at 48 min and 88 min after the first earthquake (Figure 10e, f).

Figure 11. shows snapshots of tsunami propagation simulation using hypothetical bathymetry. In this scenario, the transmitted tsunami waves were similar to those simulated using the actual bathymetry (Figure 11a, b). This similarity appeared because the source region was located in the open ocean with sea depths greater than 500 m. The first wave crest propagated toward the coast, and was amplified in association with the effect of wave shoaling in the nearshore region. However, starting at 18 min, the reflected wave from the coast was no longer trapped (Figure 11c). The reflected wave radiated homogeneously from the coast (Figure 11d). The wave was either transmitted back to the open ocean or propagated to the eastern coast (Figure 11e). This wave spread out from the coast at a relatively fast speed, and disappeared from the model domain after 88 min (Figure 11f). From the comparison, the long-lasting tsunami wave along the western coast, as shown in the real bathymetric scenario, could be attributed to wave trapping by the local bathymetry in front of southern Taiwan connected to the iteration of wave reflection and refraction.

https://doi.org/10.5194/nhess-2022-126
Preprint. Discussion started: 27 April 2022

Figure 12. shows the simulated tsunami amplitudes at all three tide gauge stations, calculated using actual and hypothetical bathymetry. With the hypothetical bathymetry (Figure 12b), the first wave crest simulated at all stations was consistently shown as the highest wave, and the amplification of the tsunami wave was absent. Additionally, from the actual bathymetric scenario (Figure 12a), the simulated tsunami waveforms after 90 min were significantly higher than those simulated using the hypothetical bathymetry. These results further confirmed that the wave trapped in southern Taiwan was related to the bathymetric effect, which could explain why Kaohsiung and Dongkung stations did not record the first wave crest as the largest, and why the tsunami oscillation recorded at Kaohsiung and Houbihu stations was prolonged.

5.3 Influence of edge waves and long-lasting tsunami hazards

As described in Section 5.2, the tsunami wave was trapped over the continental shelves and transmitted at the shelf edges along the western coast during the 2006 tsunami. The wide continental shelf along the western coast is illustrated in Figure 13a. Based on the simulated results, the maximum tsunami wave heights were distributed along the western coast, as shown in Figure 13b. This section studies how tsunami waves behaved as the edge waves, and to what extent such wave fluctuations influenced the decay of tsunami wave energy. The tsunami wave measured from point A to point D along a contour line of 20 m depth is presented in a time-distance diagram, as shown in Figure 14a.

From the time-distance diagram of the tsunami wave, the initial wave crest reached point C after 15 min, propagated along the coastline from point C to point A, and then reflected back to point C after arriving at point A at 90 min. The wave reflected iteratively between point A and point C. This process occurred because point A and point C were both located close to the cape, where the topography changed dramatically (Figure 13a). Based on the phase shift of the tsunami wave, the propagation path and travel time curves of the edge wave can be illustrated (i.e., green dashed line in Figure 14a). Based on the travel time curves of tsunami waves, the propagation speed was estimated as 33.3 m s^{-1}. The coupling of the trapped wave and the later incoming incident wave resulted in wave amplification after the arrival of first wave (i.e., spatiotemporal points indicated by black arrows in Figure 14a).

In addition, the spatiotemporal variation in tsunami wave energy along the coast of southern Taiwan was determined and plotted based on the simulated tsunami waveforms, as shown in Figure 14b. The tsunami wave energy was determined assuming that the energy flux of the tsunami wave progressed in a free sea surface region. This method was similar to that used in the study by Koyano et al., 2020. The equation of wave energy at each time step is defined as follows:

$$E\,(t) = \int_0^s \frac{1}{2}\,\rho g \eta^2(s,t)\,ds \qquad (9)$$

In this equation, E(t) is the wave energy at distances of the free sea surface at time step t, s is the distance between neighboring measurement points, ρ is the water density of the sea, g is the gravity acceleration

https://doi.org/10.5194/nhess-2022-126
Preprint. Discussion started: 27 April 2022

and is set as 9.81 m s^{-2}, t is the time step, and $\eta(s,t)$ represents the sea surface elevation of time step t. The temporal wave energy at unit area was calculated based on simulated tsunami waveforms output every 5 km along the contour line from point A to point D. To examine the decreasing tendency of tsunami wave energy at each unit area, the temporal wave energy was calculated to a total elapsed time of 300 min and was normalized as a ratio of the maximum wave energy in the time history. The normalized time-distance diagram of tsunami wave energy is plotted and shown in Figure 14c.

According to the spatiotemporal distribution of normalized wave energy, the tsunami wave energy calculated in the area between point A and point C achieved its greatest value when the first wave arrived. However, this high-energy channel did not decrease with time after the first wave arrived, instead, a persisting channel of strong energy was visible. This energy channel lasted for more than 120 min, and the wave energy repeatedly reached the maximum value in this channel. Beyond this long-lasting energy channel, the energy commenced to decrease with a relatively slow rate of energy loss at 120 min after the earthquake time. For instance, the tsunami wave energy decreased to only 80% after 135 min, and to 40% after 250 min. Accordingly, the tsunami decay process in this region was expected to last for more than 300 min. These results confirmed that the wave amplification and prolonged oscillation were connected to wave trapping and influence of edge waves. According to the occurrence of these tsunami behaviors, southern Taiwan could be affected by intensified coastal hazards and severe impacts from tsunamis due to the special coastal bathymetric features.

6. Conclusions

6.1 Main findings

In this article, the characteristics of the consecutive tsunamis on 26 December 2006, and the resulting tsunami behaviors in southern Taiwan were investigated and clarified. The methodology comprised analyses of tide gauge tsunami waveforms, spectral analyses and numerical tsunami simulations. The main findings are summarized as follows:

(1) The physical characteristics of tsunami waveforms in all three tide gauge stations in southern Taiwan during the December 2006 tsunami were characterized. The initial tsunami wave arrived at Kaohsiung, Dongkung, and Houbihu at Taiwan standard times of 21:18, 20:54, and 20:42, respectively, with a trough sign of tsunami amplitude. Following the initial wave trough, the initial wave crests were 0.07 m (Kaohsiung), 0.09 m (Dongkung), and 0.3 m (Houbihu). The maximum tsunami wave heights at the three tide gauge stations at Kaohsiung, Dongkung, and Houbihu were 0.08 m, 0.12 m, and 0.3 m, respectively, and the maximum tsunami wave heights at Kaohsiung and Dongkung were not recorded with the first arrivals. The approximate tsunami duration in Dongkung was 3.9 h, while the tsunami lasted for more than 6 h in Kaohsiung and Houbihu.

(2) Based on the spectral analyses of tsunami waveforms, the period band of 15.5-26.6 min was attributed to the tsunami source spectrum, and the approximate source area for the consecutive tsunamis was

https://doi.org/10.5194/nhess-2022-126
Preprint. Discussion started: 27 April 2022


Natural Hazards and Earth System Sciences
Discussions

estimated to be 800 km^2. Other dominant periods such as 30 min, 36 min, and 60 min could be interpreted as periodic components contributed by non- source phenomena, such as shelf resonance.

(3) The earthquake tsunami scenarios were validated based on simulated results, and compared to the observations at all three CWB tide gauge stations in southern Taiwan. The validation of the numerical results revealed that the fault geometries of the GCMT model could explain the tsunami sources of the consecutive earthquakes in terms of tsunami waveforms better those of the USGS model.

(4) The comparison of tsunami propagation as simulated using actual and hypothetical bathymetric scenarios revealed that the wave trapping around southern Taiwan during the passage of the 2006 tsunami was associated with the wave refraction caused by coastal bathymetry. The trapped tsunami waves reflected iteratively and interfered with the incident waves at the boundaries of shelves, which resulted in wave amplification and prolonged oscillation connected to shelf resonance. This process explained why some observations recorded at tide gauge stations during the 2006 tsunami were contradictory with respect to the common sequences of near-field tsunamis.

(5) Tsunami are one of the most dangerous coastal hazards and can cause destructive damage and loss of life in coastal regions. Taiwan is one of the countries at risk of tsunamis and is exposed to potential near-field tsunamis expected to be generated from the Manila Trench on the South China Sea (SCS) side and the Ryukyu Trench on Pacific Ocean side. The results of the present study revealed that the tsunami wave was trapped over the insular shelves around southern Taiwan during the passage of the tsunami. The long-lived edge waves and resonant features might result in unexpected amplification of tsunami heights and long tsunami durations in southern Taiwan. In other words, even if the initial wave heights are small, the tsunami waves that arrived later are expected to be higher and more persistent along the coast of southern Taiwan. Therefore, decision makers and people in southern Taiwan should be aware and stay clear of coastal regions for a long time as an emergency response to future tsunamis, even though the wave height of the initially arriving tsunami wave is small. Moreover, the present study provides an understanding of previously unidentified tsunami hazards in southern Taiwan, which are important and valuable for improving existing tsunami warnings and coastal planning for disaster risk management.

6.2 Limitations and future improvements

In this study, the characteristics of the December 2006 tsunami and resulting tsunami behaviors in southern Taiwan were explored using available data from tide gauge tsunami waveforms and numerical tsunami simulations. Nevertheless, it is noteworthy that the analyses in this article have some limitations. The first limitation is related to the tsunami data recorded at the tide gauge stations, which were employed as input data for spectral analyses (i.e., Fourier analyses and wavelet analyses) and comparison with the numerical results. The sampling interval of the tide gauge data recorded at all CWB tide gauge stations was 6 min, indicating that tsunami wave components with shorter periods might not be well recorded in the tide

https://doi.org/10.5194/nhess-2022-126
Preprint. Discussion started: 27 April 2022

gauge data. Due to this existing limitation, spectral analyses might cause discrepancies in detecting periodic components of tsunami spectra. This limitation could be improved, including the use of tsunami data with frequent sampling rate.

Another limitation was related to the simulation grid size (i.e., 450 m) for tsunami propagation simulation. Although the simulated tsunami waveforms were reasonably consistent with the observed values recorded at the tide gauge stations in terms of wave amplitude and arrival time for model validation, the frequency of the tsunami waveforms was not well resolved because of the coarse bathymetric grid. The reproducibility of numerical results for the 2006 tsunami could be further improved, including making a finer grid of bathymetric data available. In addition, tsunami waveforms in the later phase may not be well simulated because the numerical model adopted in this article was based on the nonlinear theory of the shallow water equation. For a better solution of the later wave phase, wave dispersion theory (i.e., for instance, the Boussinesq wave equation) should be considered and included in the numerical model to accurately simulate tsunami propagation.

All limitations mentioned above suggest further improvements to research to provide a more detailed investigation of issues of long-lived edge waves and shelf resonance, especially in the region of southern Taiwan. In addition, more fundamental studies on the complex wave mechanisms of tsunami reflection and refraction, shoaling effects, and wave trapping by insular shelves are planned for future work.

Acknowledgements.

This work used recorded sea level data from tide gauge stations, which are maintained by the Central Weather Bureau (CWB), R.O.C. The bathymetric data used for numerical tsunami simulations are available from the General Bathymetric Chart of the Oceans (GEBCO), 2021. The seismic information is available in publicly-accessible catalogs of the Global Centroid Moment Tensor Project (GCMT) and United States Geological Survey (USGS), as mentioned in the body of the article. We appreciate Ms. Shyh-Fang Liu and Ms. Cheng-Lin Huang for their great support in collecting the observation record data used in this work. This work was supported (in part) by the MEXT WISE Program for Sustainability in the Dynamic Earth.

References

Cheng, S., Shaw, C., and Yeh, Y., Reconstructing the 1867 Keelung Earthquake and Tsunami Based on Historical Documents, Terr. Atmos. Ocean. Sci., Vol. 27, No. 3, 431-449, June 2016

Hayashi, Y., Koshimura, S., and Imamura, F., Comparison of decay features of the 2006 and 2007 Kuril Island earthquake tsunamis, Geophys. J. Int. (2012) 190, 347-357

Heidarzadeh, M., and Satake, K., Waveform and spectral analyses of the 2011 Japan tsunami records on tide gauge and DART stations across the Pacific Ocean, Pure Appl. Geophys., 170, 1275–1293, doi:10.1007/s00024- 012-0558-5, 2013.

https://doi.org/10.5194/nhess-2022-126
Preprint. Discussion started: 27 April 2022

Heidarzadeh, M., Harada, T., Satake, K., Ishibe, T., and Gusman, A. R., Comparative study of two tsunamigenic earthquakes in the Solomon Islands: 2015 Mw 7.0 normal-fault and 2013 Santa Cruz Mw 8.0 megathrust earthquakes, Geophys. Res. Lett., 43, 4340–4349. doi:10.1002/2016GL068601, 2016.

Heidarzadeh, M., Muhari, A., and Wijanarto, A., Insight on the Source of the 28 September 2018 Sulawesi Tsunami, Indonesia Based on Spectral Analyses and Numerical Simulation, Pure Appl. Geophys., 176, 25-43, https://doi.org/10.1007/s00024-018-2065-9

Harris, C. R., Millman, K. J., van der Walt, S. J., Gommers, R., Virtanen, P., Cournapeau, D., … Oliphant, T. E. (2020). Array programming with NumPy. Nature, 585, 357–362. https://doi.org/10.1038/s41586-020-2649-2

Heidarzadeh, M., Pranantyo, I., Okuwaki, R., Dogan, G., and Yalciner, A., Long Tsunami Oscillations Following the 30 October 2020 Mw7.0 Aegean Sea Earthquake: Observation and Modelling, Pure Appl. Geophys.,1531-1548, https://doi.org/10.1007/s00024-021-02761-8

Imamura, F.: Review of tsunami simulation with a finite difference method, Long-Wave Runup Models, World Scientific, 25–42, 1995.

Kotani, M., Imamura, F. & Shuto, N. (1998) Tsunami run-up simulation and damage estimation by using GIS. Proceedings of Coastal Engineering, JSCE, 45, 356-360.

Koyano, K., Takabatake, T., Esteban, M., Shibayama, T., ASCE, M., Influence of Edge Waves on Tsunami Characteristics along Kujukuri Beach, Japan, Journal of Waterway, Port, Coastal, and Ocean Engineering, doi: 10.1061/(ASCE)WW.1943-5460.0000617.

Lay, T., and Kanamori, H., EARTHQUAKE DOUBLET IN THE SOLOMON ISLANDS, Physics of the Earth and Planetary Interiors, 21 (1980) 283-304

Li, L., A. D. Switzer, Y. Wang, R. Weiss, Q. Qiu, C.-H. Chan, and P. Tapponnier (2015), What caused the mysterious eighteenth century tsunami that struck the southwest Taiwan coast?, Geophys. Res. Lett., 42, 8498–8506, doi:10.1002/2015GL065567.

Li, L., A. D. Switzer, C.-H. Chan, Y. Wang, R. Weiss, and Q. Qiu (2016), How heterogeneous coseismic slip affects regional probabilistic tsunami hazard assessment: A case study in the South China Sea, J. Geophys. Res. Solid Earth, 121, 6250–6272, doi:10.1002/2016JB013111.

Liu, L., Wang, X., and Salisbury, A., Tsunami hazard and early warning system in South China Sea, Journal of Asian Earth Science, 36 (2009) 2-12

Masaya, R., Suppasri, A., Yamashita, K., Imamura, F., Gouramanis, C., and Leelawat, N., Investigating beach erosion related with tsunami sediment transport at Phra Thong Island, Thailand, caused by the 2004 Indian Ocean Tsunami, Nat. Hazards Earth Syst. Sci., 20, 2823–2841, 2020, https://doi.org/10.5194/nhess-20-2823-2020

Megawati, K., Shaw, F., Sieh, K., Huang, Z., Wu, T., Lin, Y., Tan, S., Pan, T., Tsunami hazard from the subduction megathrust of the South China Sea: Part 1. Source characterization and the resulting tsunami, Journal of Asian Earth Science 36 (2009) 13-20

https://doi.org/10.5194/nhess-2022-126
Preprint. Discussion started: 27 April 2022

Okada, Y., Surface deformation due to shear and tensile faults in a half-space, Bull. Seismol. Soc. Am., 75(4), 1135–1154, 1985.

Okal, E. A., Synolakis, C. E. and Kalligeris, N.: Tsunami simulations for regional sources in the South China and adjoining seas, Pure. Appl. Geophys., 168(6), 1153–1173, doi: 10.1007/s00024-010-0230-x, 2011.

Papazachos, B., Scordilis, E., Panagiotopoulos, D., Papazachos, C., Karakaisis, G., Global relations between seismic fault parameters and moment magnitude of earthquakes, Bull. Geol. Soc. Greece XXXVI (2004) 1482-1489

Qiu, Q., Li, L., Hsu, Y., Wang, Y., Chan, C., and Switzer, A., Revised earthquake sources along Manila trench for tsunami hazard assessment in the South China Sea, Nat. Hazards Earth Syst. Sci., 19, 1565–1583, 2019 https://doi.org/10.5194/nhess-19-1565-2019

Rabinovich, A., Spectral analysis of tsunami waves: Separation of the source and topography effects, JOURNAL OF GEOPHYSICAL RESEARCH, VOL. 102, NO. C6, PAGES 12,663-12,676, JUNE 15, 1997

Rabinovich, A., Candella, R., and Thomson, R., The open ocean energy decay of the three recent trans-Pacific tsunamis, GEOPHYSICAL RESEARCH LETTERS, VOL. 40, 3157-3162, doi: 10.2002/grl.50625, 2013

Roeber, V., Yamazaki, Y., and Cheung, K., Resonance and impact of the 2009 Samoa tsunami around Tutuila, American Samoa, GEOPHYSICAL RESEARCH LETTERS, VOL. 37, L21604, doi: 10.1029/2010GL044419, 2010

Sugawara, D., Yu, N., and Yen, J., Estimating a Tsunami Source by the Sediment Transport Modeling: A Primary Attempt on a Historical/ 1867 Normal-Faulting Tsunami in Northern Taiwan, Journal of Geophysical Research: Earth Surface, 124, 1675–1700. https://doi.org/10.1029/2018JF004831

Sun, Y.-S., Chen, P.-F., Chen, C.-C., Lee, Y.-T., Ma, K.-F., and Wu, T.-R.: Assessment of the peak tsunami amplitude associated with a large earthquake occurring along the southernmost Ryukyu subduction zone in the region of Taiwan, Nat. Hazards Earth Syst. Sci., 18, 2081–2092, https://doi.org/10.5194/nhess-18-2081-2018, 2018.

Sugawara D. (2018) Evolution of Numerical Modeling as a Tool for Predicting Tsunami-Induced Morphological Changes in Coastal Areas: A Review Since the 2011 Tohoku Earthquake. In: Santiago-Fandiño V., Sato S., Maki N., Iuchi K. (eds) The 2011 Japan Earthquake and Tsunami: Reconstruction and Restoration. Advances in Natural and Technological Hazards Research, vol 47. Springer, Cham. https://doi.org/10.1007/978-3-319-58691-5_26

Suppasri, A., Fukutani, T., Tabuchi, S., Imamura, F., Mapping of historical tsunamis in the Indian and Southwest Pacific Oceans, International Journal of Disaster Risk Reduction1 (2012) 62-71,

Suppasri, A., Muhari, A., Fukutani, T., Imamura, F., and Shuto, N., Loss Functions for Small Marine Vessels Based on Survey Data and Numerical Simulation of the 2011 Great East Japan Tsunami, Journal of Waterway, Port, Coastal, and Ocean Engineering, doi: 10.1061/(ASCE)WW.1943-5460.0000244

https://doi.org/10.5194/nhess-2022-126
Preprint. Discussion started: 27 April 2022

635 Suppasri, A., Leelawat, N., Latcharote, P., Roeber, V., Yamashita, K., Hayashi, A., Ohira, H., Fukui, K., Hisamatsu, A., Nguyen, David, Imamura, F., The 2016 Fukushima earthquake and tsunami: Local tsunami behavior and recommendations for tsunami disaster risk reduction, International Journal of Disaster Risk Reduction 21 (2017) 323-330

Suppasri, A., Maly, E., Kitamura, M., Syamsidik, Pescaroli. G., Alexander, D., Imamura, F., Cascading 640 disasters triggered by tsunami hazards: A perspective for critical infrastructure resilience and disaster risk reduction, International Journal of Disaster Risk Reduction66 (2021) 1002597

Tanioka, Y., and Satake, K., Tsunami generation by the horizontal displacement of the ocean bottom, GEOPHYSICAL RESEARCH LETTERS, VOL. 23, NO. 8, PAGES 861-864, APRIL 15, 1996

Torrence, C., and Compo, G., A practical guide to wavelet analysis, Bull. Am. Meteorol. Soc., 79, 61–78, 645 doi:10.1175/1520- 0477(1998)0792.0.CO;2, 1998.

Toguchi, Y., Fujii, S., & Hinata, H. (2018), Tsunami waves and tsunami-induced natural oscillations determined by HF radar in Ise Bay, Japan. Journal of Geophysical Research: Oceans, 123, 2965–2980. https://doi.org/10.1029/2017JC013626

Wang, Y., Zamora, N., Quiroz, M., Satake, K., & Cienfuegos, R. (2021). Tsunami resonance 650 characterization in Japan due to trans-Pacific sources: Response on the bay and continental shelf. Journal of Geophysical Research: Oceans, 126, e2020JC017037. https://doi.org/10.1029/2020JC017037

Wu, T., and Huang, H., Modeling tsunami hazards from Manila trench to Taiwan, Journal of Asian Earth Science 36 (2009) 21-78

Wu, T., Chen, P., Tsai, W., Chen, G., Numerical Study on Tsunami Excited by 2006 Pingtung Earthquake 655 Doublet, Terr. Atmos. Ocean. Sci., Vol. 19, No. 6, 705-715, December 2008

Wu, Y., Zhao, L., Chang, C., Hsiao, N., Chen, Y., and Hsu, S., Relocation of the 2006 Pingtung Earthquake sequence and seismotectonics in Southern Taiwan, Tectonophysics 479 (2009) 19-27

National Disaster Prevention and Protection Commission, R.O.C., 2007. Statistics on the Losses on Natural Disaster. http://www.ndppc.nat.gov.tw/.

660 Yamazaki, Y., and Cheung, L., Shelf resonance and impact of near-field tsunami generated by the 2010 Chile earthquake, GEOPHYSICAL RESEARCH LETTERS, VOL. 38, L12605, doi:10.1029/2011GL047508, 2011

https://doi.org/10.5194/nhess-2022-126
Preprint. Discussion started: 27 April 2022

Natural Hazards and Earth System Sciences
Discussions
Open Access
EGU

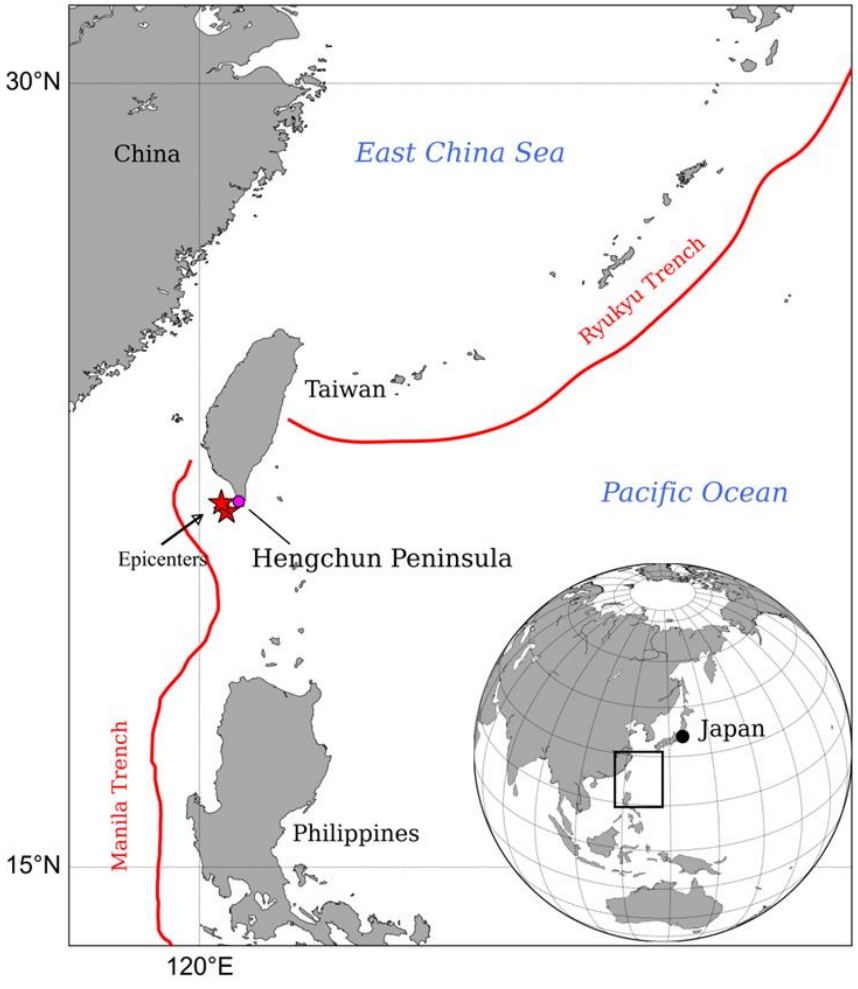

665 **Figure 1. Map of location of the Hengchun Peninsula, Taiwan. The red star symbols illustrate the epicenters of doublet earthquakes, and red solid lines illustrate the subduction zones of the Manila Trench and the Ryukyu Trench.**

https://doi.org/10.5194/nhess-2022-126
Preprint. Discussion started: 27 April 2022

Natural Hazards and Earth System Sciences
Discussions

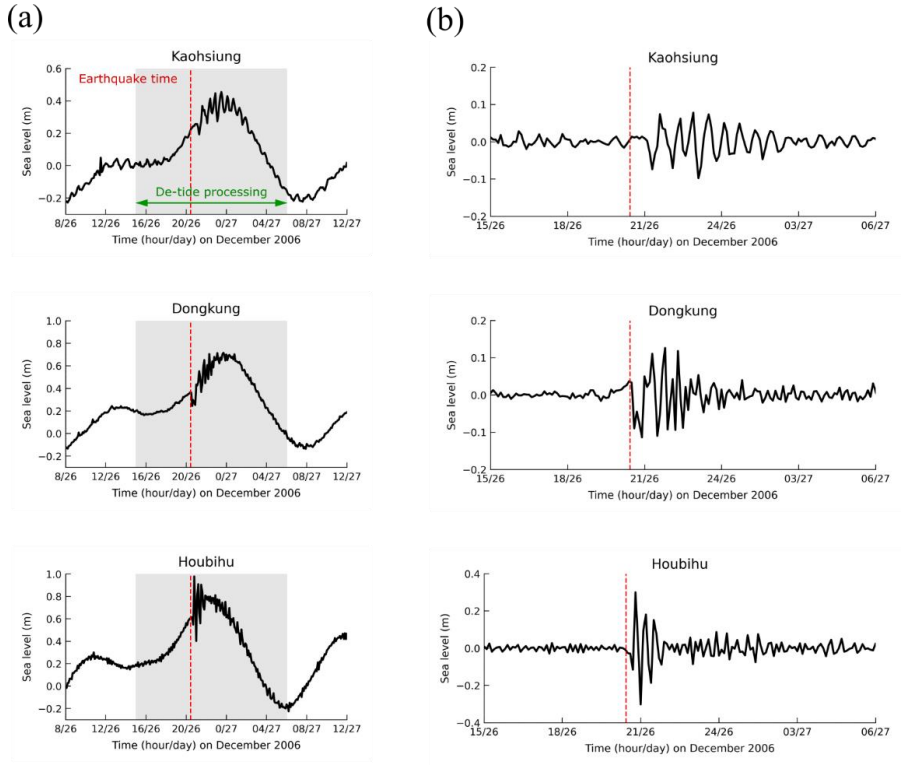

Figure 2. The (a) original and (b) de-tided sea levels recorded at tide gauge stations in southern Taiwan during the 26 December 2006 tsunami event. The vertical red dashed lines indicate the occurrence of the first earthquake. The gray shaded areas illustrate the portion of original data input for detide processing. The data shown in the graphs were drawn based on Taiwan standard time.

https://doi.org/10.5194/nhess-2022-126
Preprint. Discussion started: 27 April 2022

Natural Hazards and Earth System Sciences
Discussions

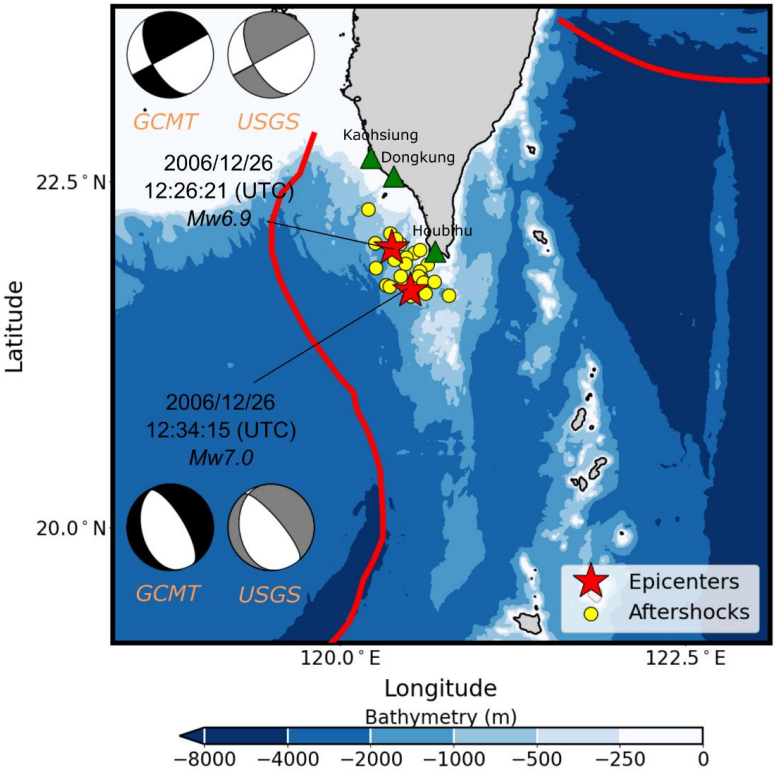

675

Figure 3. Maps of the tectonic settings and bathymetric data of the model domain. The red stars denote the epicenters of two successive earthquakes and the beach-balls illustrate the focal mechanisms of the doublet earthquakes given by the moment tensor as solved by the GCMT and USGS. The yellow circles show the aftershock distribution for one day from the USGS earthquake catalog. The green triangles represent the

680 **locations of the CWB tide gauge stations. The red solid lines illustrate the subduction zone systems of the Manila Trench and the Ryukyu Trench, located offshore Taiwan.**

https://doi.org/10.5194/nhess-2022-126
Preprint. Discussion started: 27 April 2022

Natural Hazards and Earth System Sciences
Discussions

Table 1. Parameters of the focal mechanisms for doublet earthquakes, solved by GCMT and USGS.

	Seismological agency			
	GCMT		USGS	
	Eq1	Eq2	Eq1	Eq2
Moment magnitude (M_w)	7.0	6.9	7.0	6.9
Earthquake time (UTC)	12:26:21	12:34:15	12:26:21	12:34:15
Longitude (° E)	120.52	120.40	120.55	120.50
Latitude (° N)	21.81	22.02	21.80	21.97
Depth (km)	19.6	32.8	25.5	32.8
Strike (degree)	165	151	171	151
Dip (degree)	30	48	24	48
Rake (degree)	-76	0	-61	0

685

https://doi.org/10.5194/nhess-2022-126
Preprint. Discussion started: 27 April 2022

Natural Hazards and Earth System Sciences
Discussions

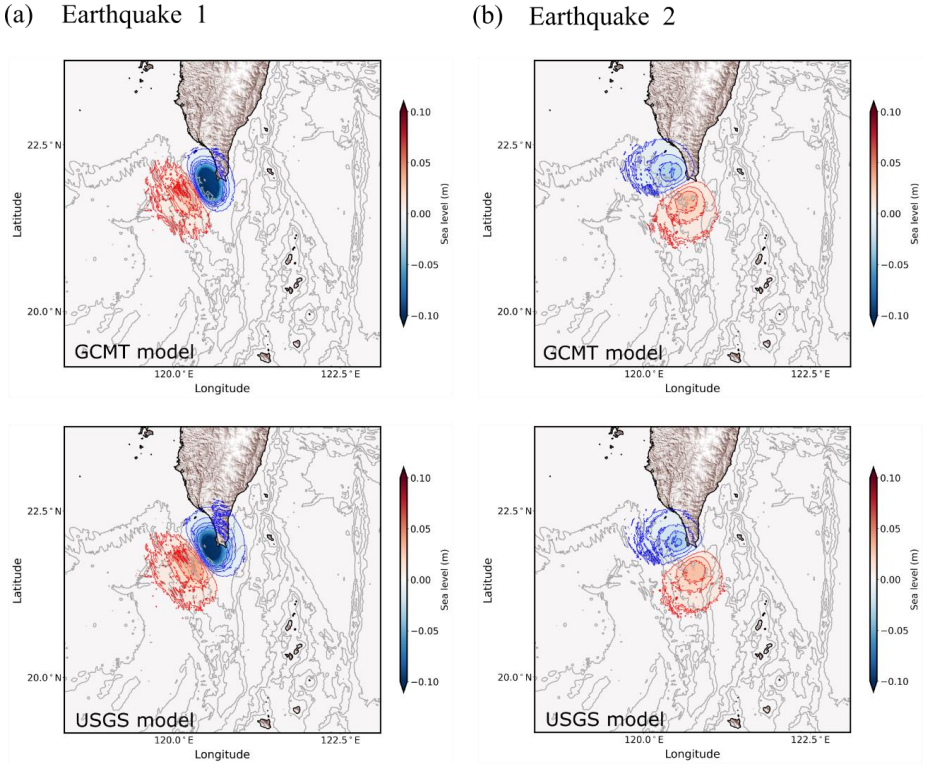

Figure 4. Distributions of initial sea surface elevations due to the doublet earthquakes of the (a) first (12:26:21, UTC) and (b) second earthquakes (12:34:15, UTC) calculated using the GCMT and USGS models of fault geometries. The bathymetric contours are drawn every 1000 m.

690

https://doi.org/10.5194/nhess-2022-126
Preprint. Discussion started: 27 April 2022

Natural Hazards and Earth System Sciences
Discussions
Open Access
EGU

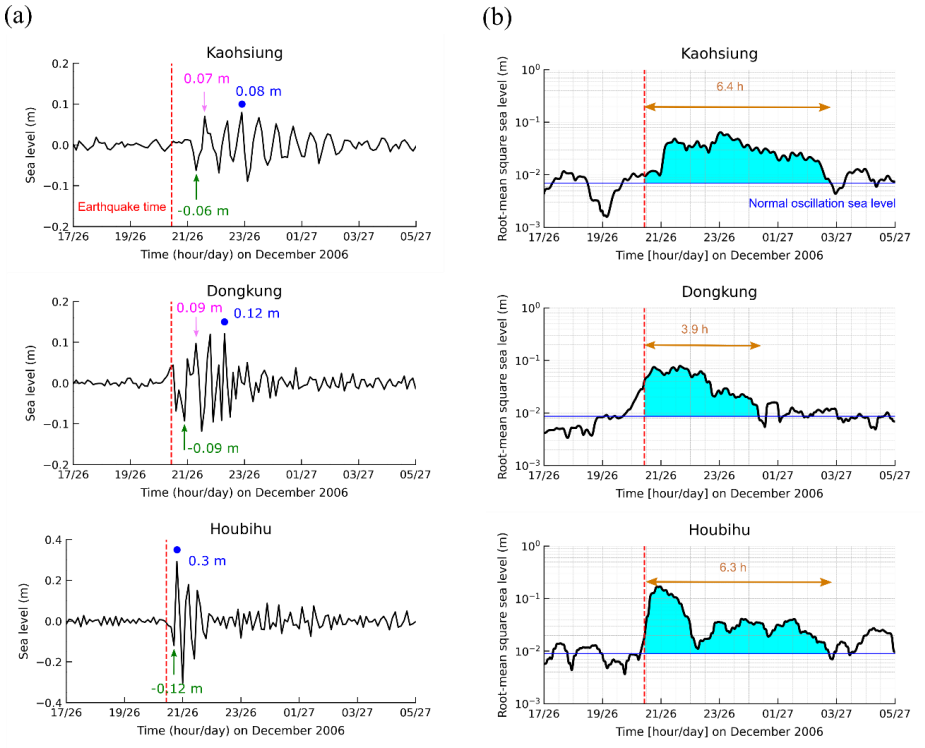

Figure 5. (a) The recorded of tsunami waveforms, and (b) diagrams of root-mean-square (RMS) sea levels of the 2006 Hengchun tsunami at the Kaohsiung, Dongkung, and Houbihu tide gauge stations. The vertical red dashed lines indicate the original earthquake time of first earthquake. The blue circles denote the arrival of the maximum crest wave recorded at all sites. The pink arrows mark the first wave crest. The green arrows represent the trough sign of the first wave arrival. The blue solid lines represent the normal oscillation level before the tsunami arrived (i.e., the mean value of sea level before original earthquake time). The high-energy tsunami wave is illustrated in cyan blue-shaded areas. The orange arrows show the elapsed time of tsunami duration.

https://doi.org/10.5194/nhess-2022-126
Preprint. Discussion started: 27 April 2022

Natural Hazards and Earth System Sciences
Discussions

Table 2a. Details of tide gauge stations and physical characteristics of tsunami waveforms during the 2006 tsunami.

Station	Longitude (°E)	Latitude (°N)	Wave amplitude (m)		
			First trough sign	First wave crest	Maximum wave crest
Kaohsiung	120.28	22.61	-0.06	0.07	0.08
Dongkung	120.43	22.46	-0.09	0.09	0.12
Houbihu	120.74	21.94	-0.12	0.3	0.3

Table 2b. Details of tide gauge stations and physical characteristics of tsunami waveforms during the 2006 tsunami.

Station	Arrival time (Taiwan standard time)			Delay of maximum wave crest (min)	Visible period (min)
	First trough sign	First wave crest	Maximum wave crest		
Kaohsiung	21:18	21:44	22:54	70	30-48
Dongkung	20:54	21:18	22:18	60	18-24
Houbihu	20:42	20:48	20:48	0	18-24

https://doi.org/10.5194/nhess-2022-126
Preprint. Discussion started: 27 April 2022

Natural Hazards and Earth System Sciences
Discussions

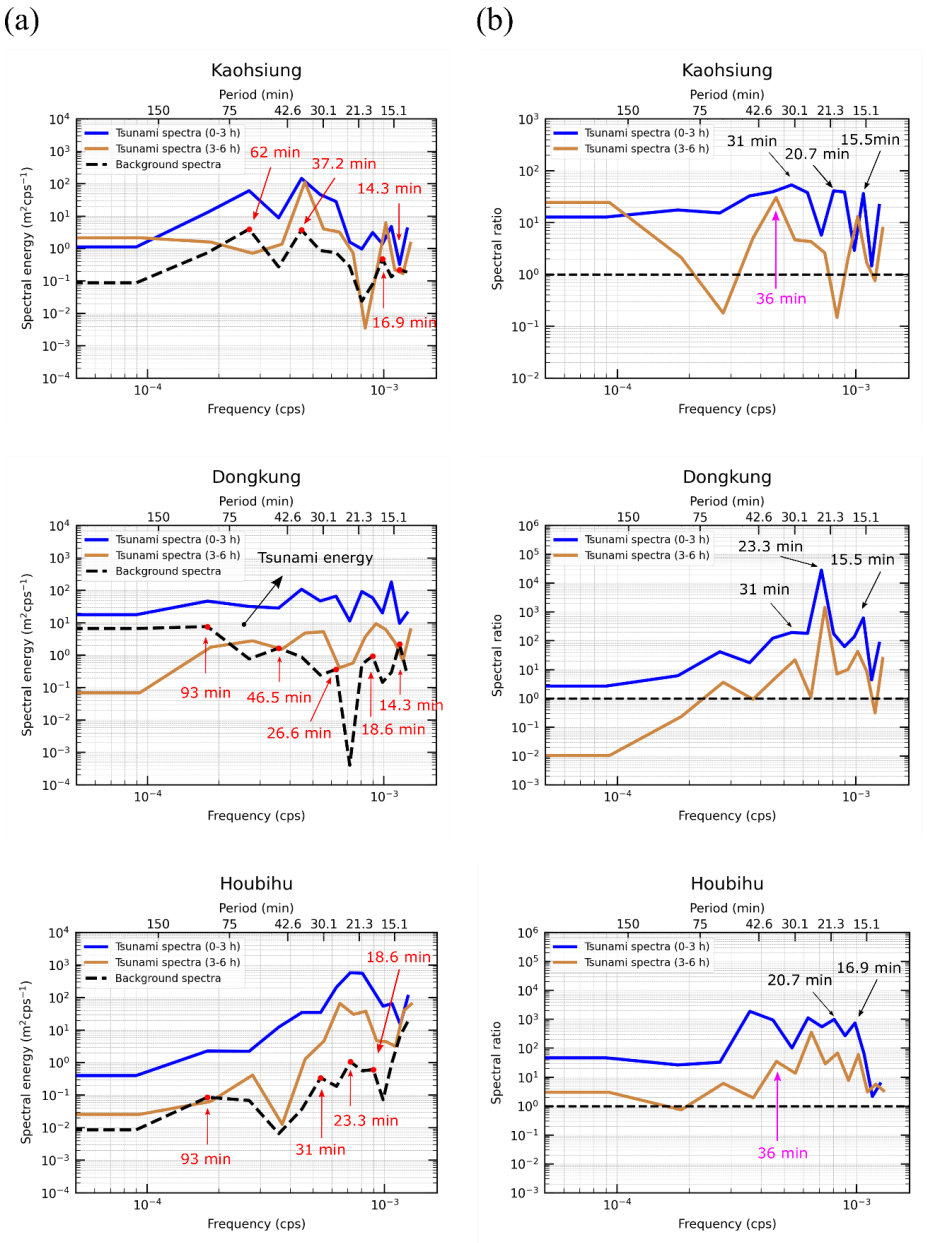

Figure 6. (a) The tsunami (blue and yellow solid lines) and background spectra (black dashed lines) and (b) the spectral ratios of tsunami data for the 2006 Hengchun tsunami at tide gauge stations.

710

https://doi.org/10.5194/nhess-2022-126
Preprint. Discussion started: 27 April 2022

Natural Hazards and Earth System Sciences
Discussions

Table 3a. Details and summary of dominant periods for spectral peaks of background and tsunami signals recorded at tide gauge stations.

	Tide gauge station		
	Kaohsiung	Dongkung	Houbihu
Periods of spectral peaks for background spectra (min)	14.3	14.3	18.6
	16.9	18.6	23.3
	37.2	26.6	31.0
	62.0	46.5	93.0
		93.0	
Periods of spectral peaks for tsunami spectra of 0-3 h (min)	15.5	15.5	15.5
	18.6	20.7	23.3
	37.2	26.6	93.0
	62.0	37.2	
		93.0	
Periods of spectral peaks for tsunami spectra of 3-6 h (min)	16.3	18.0	20.0
	36.0	30.0	25.7
		60.0	60.0

Table 3b. Dominant periods of spectral ratio peaks for tsunami signals at tide gauge stations.

	Tide gauge station		
	Kaohsiung	Dongkung	Houbihu
Periods of spectra ratio peaks for tsunami signals of 0-3 h (min)	15.5	15.5	16.9
	20.7	23.3	20.7
	31	31	26.6
		62	46.5
Periods of spectra ratio peaks for tsunami signals of 3-6 h (min)	16	16.4	16.4
	36	22.5	20
		30	25.7
		60	36
			60

715

https://doi.org/10.5194/nhess-2022-126
Preprint. Discussion started: 27 April 2022

Natural Hazards and Earth System Sciences
Discussions

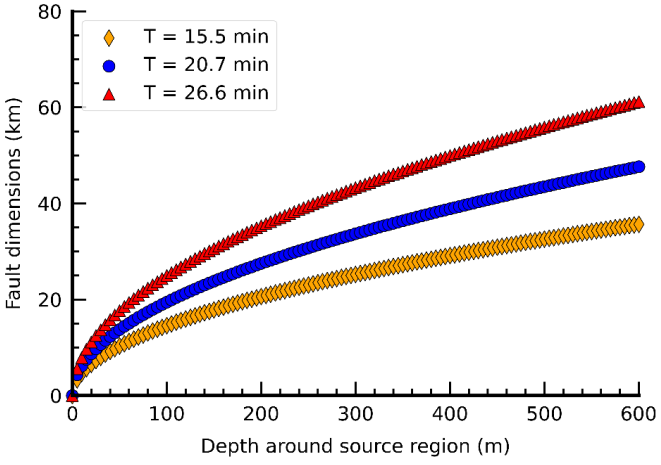

Figure 7. Correlation of earthquake fault dimensions and sea depths around the tsunami source region derived based on the empirical formula proposed by Rabinovich, 1997.

720

https://doi.org/10.5194/nhess-2022-126
Preprint. Discussion started: 27 April 2022

Natural Hazards and Earth System Sciences
Discussions

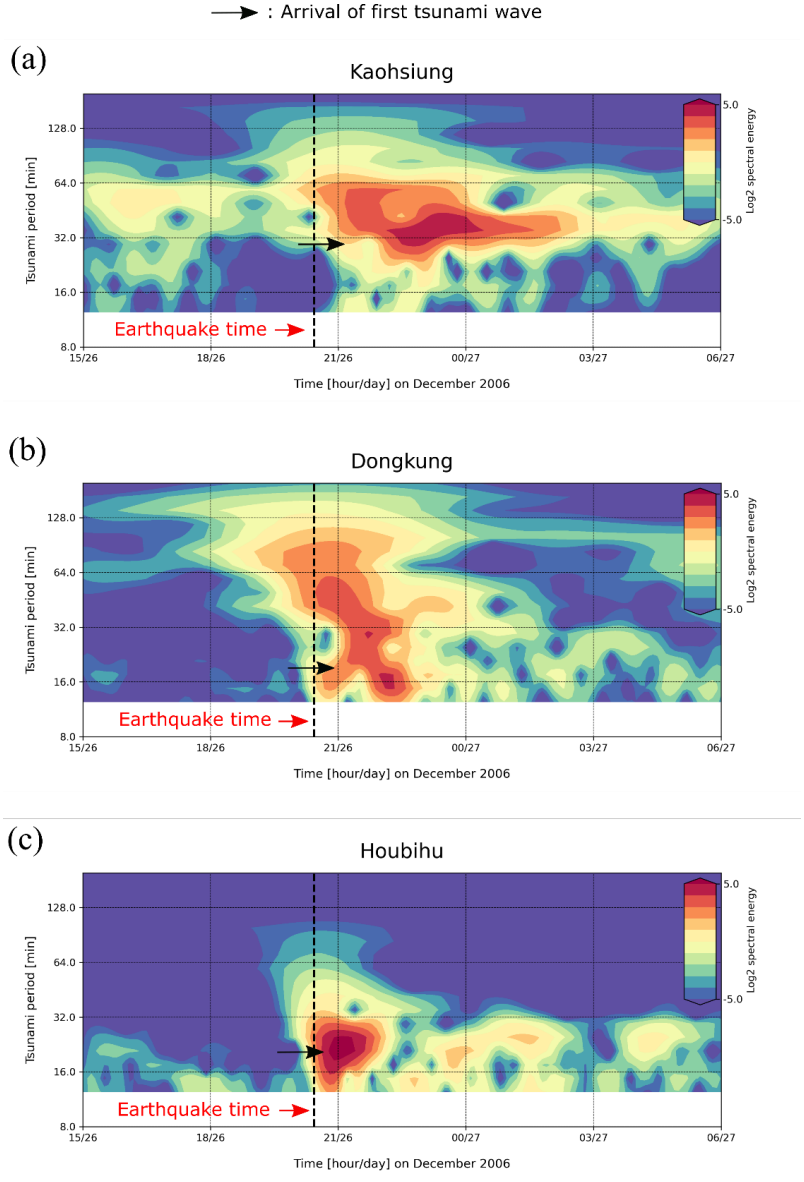

Figure 8. Wavelet (time-frequency) diagrams of tsunami data for the 26 December 2006 tsunami event at the (a) Kaohsiung, (b) Dongkung, and (c) Houbihu tide gauge stations. The colormap represents the log2 spectral energy at various times and tsunami periods. The black vertical dashed lines indicate the origin time of the first earthquake. The black arrows denote the arrival time of the first tsunami wave at each station.

https://doi.org/10.5194/nhess-2022-126
Preprint. Discussion started: 27 April 2022

Natural Hazards and Earth System Sciences
Discussions

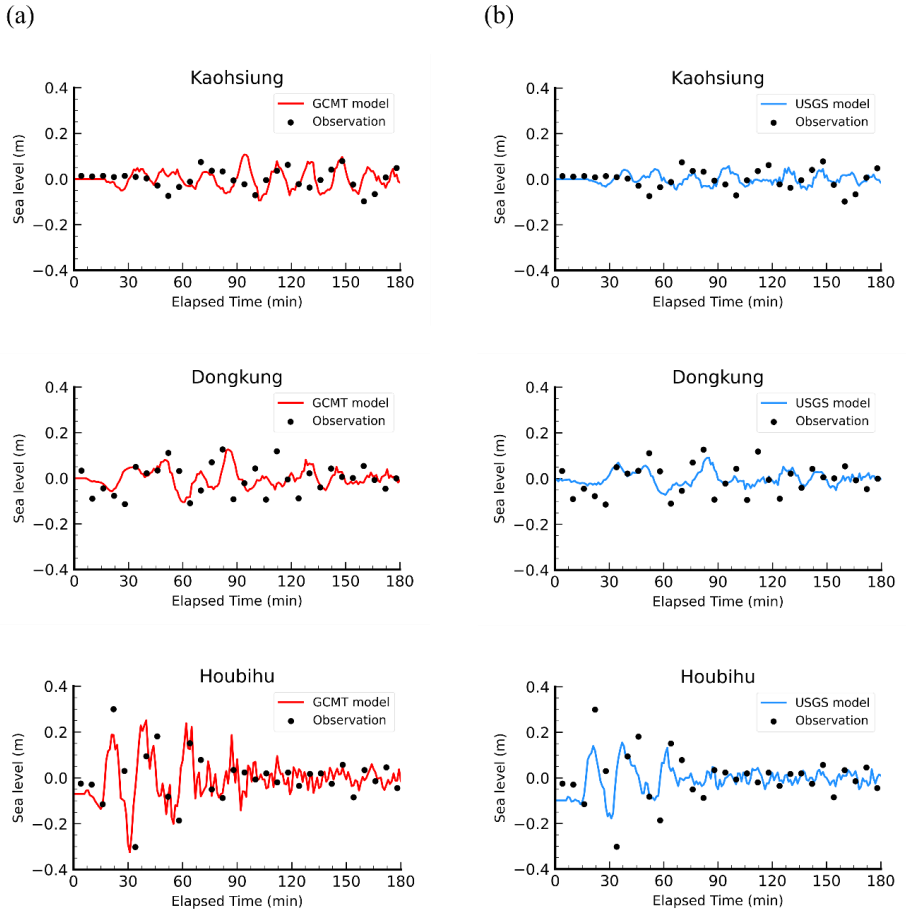

Figure 9. Comparison of simulated and observed tsunami waveforms at various tide gauge stations for the 26 December 2006 Hengchun tsunami. Solid lines illustrate simulated tsunami waveforms based on earthquake scenarios. The black solid symbols show the recorded sea level at each tide gauge at 6-min intervals.

https://doi.org/10.5194/nhess-2022-126
Preprint. Discussion started: 27 April 2022

Natural Hazards and Earth System Sciences
Discussions

Table 4a. Details of tide gauge stations for comparison of recorded and simulated wave amplitude

Station	GCMT scenario				USGS scenario			
	First wave crest (m)		Maximum wave crest (m)		First wave crest (m)		Maximum wave crest (m)	
	Recorded	Simulated	Recorded	Simulated	Recorded	Simulated	Recorded	Simulated
Kaohsiung	0.07	0.05	0.08	0.11	0.07	0.04	0.08	0.06
Dongkung	0.11	0.05	0.13	0.13	0.11	0.07	0.13	0.09
Houbihu	0.3	0.19	0.3	0.25	0.3	0.14	0.3	0.16

Table 4b. Details of tide gauge stations for comparison of recorded and simulated arrival time

Station	GCMT scenario				USGS scenario			
	First wave crest (min)		Maximum wave crest (min)		First wave crest (min)		Maximum wave crest (min)	
	Recorded	Simulated	Recorded	Simulated	Recorded	Simulated	Recorded	Simulated
Kaohsiung	70	35	148	94	70	39	148	96
Dongkung	52	50	82	82	52	35	82	85
Houbihu	22	22	22	40	22	22	22	38

735

https://doi.org/10.5194/nhess-2022-126
Preprint. Discussion started: 27 April 2022

Natural Hazards and Earth System Sciences
Discussions

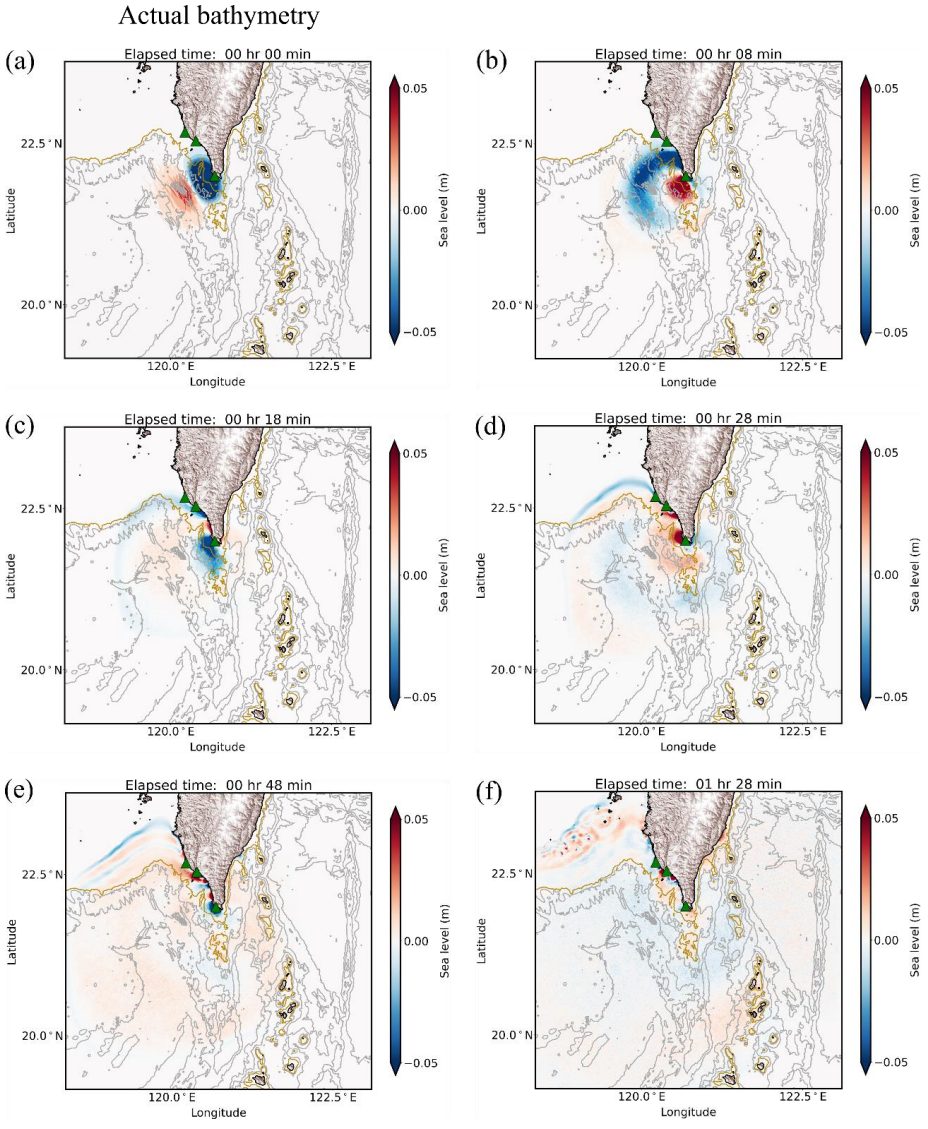

Figure 10. Snapshots of simulated tsunami propagation for the 26 December 2006 southern Taiwan tsunami using the actual bathymetry. The green triangles indicate CWB tide gauge stations. The bathymetry is plotted as gray solid lines with a contour interval of 1000 m for bathymetry deeper than 1000 m, and the 500-m contours are emphasized by the gold solid lines.

https://doi.org/10.5194/nhess-2022-126
Preprint. Discussion started: 27 April 2022

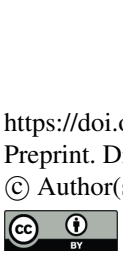

Natural Hazards and Earth System Sciences
Discussions

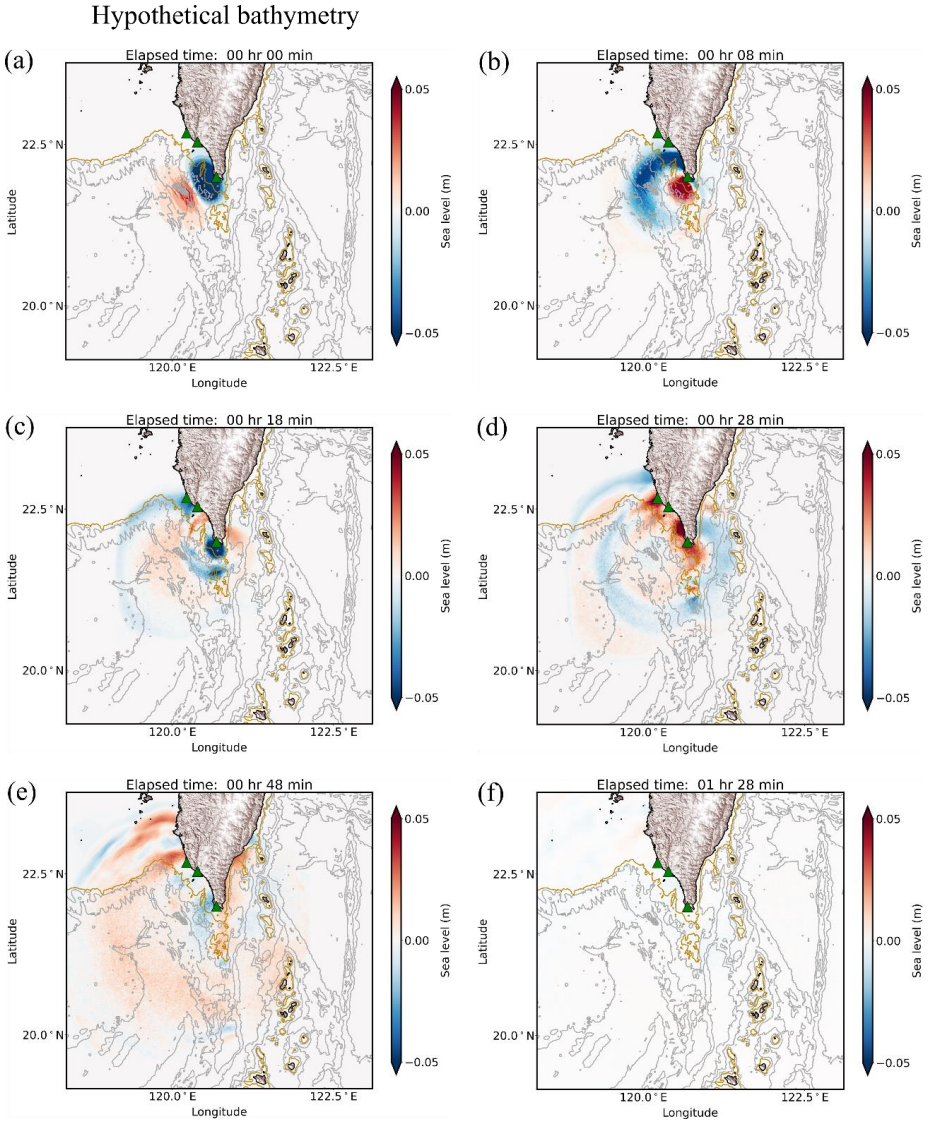

Figure 11. Snapshots of simulated tsunami propagation for the 26 December 2006 southern Taiwan tsunami using hypothetical bathymetry. The green triangles indicate CWB tide gauge stations. The bathymetry is plotted as gray solid lines with a contour interval of 1000 m for bathymetry deeper than 1000 m, and the 500-m contours are emphasized by the gold solid lines.

https://doi.org/10.5194/nhess-2022-126
Preprint. Discussion started: 27 April 2022

Natural Hazards and Earth System Sciences
Discussions

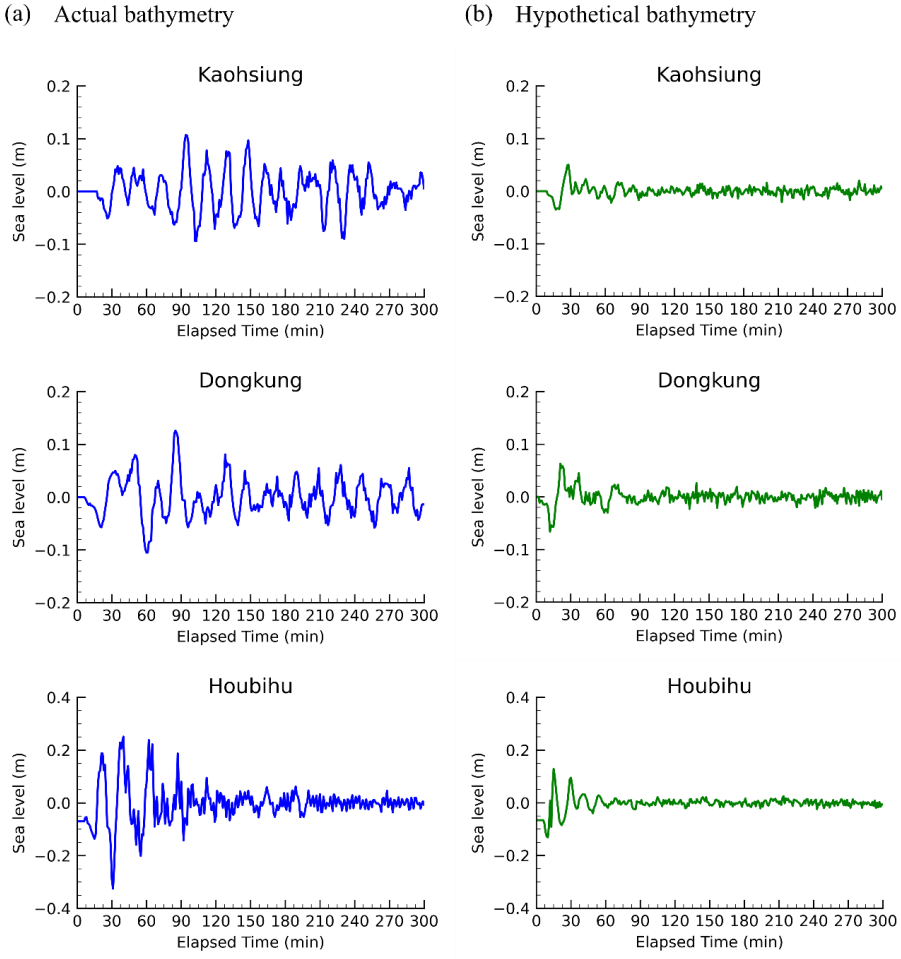

Figure 12. Comparisons of simulated tsunami waveforms, calculated using (a) actual and (b) hypothetical bathymetry.

https://doi.org/10.5194/nhess-2022-126
Preprint. Discussion started: 27 April 2022

Natural Hazards and Earth System Sciences
Discussions

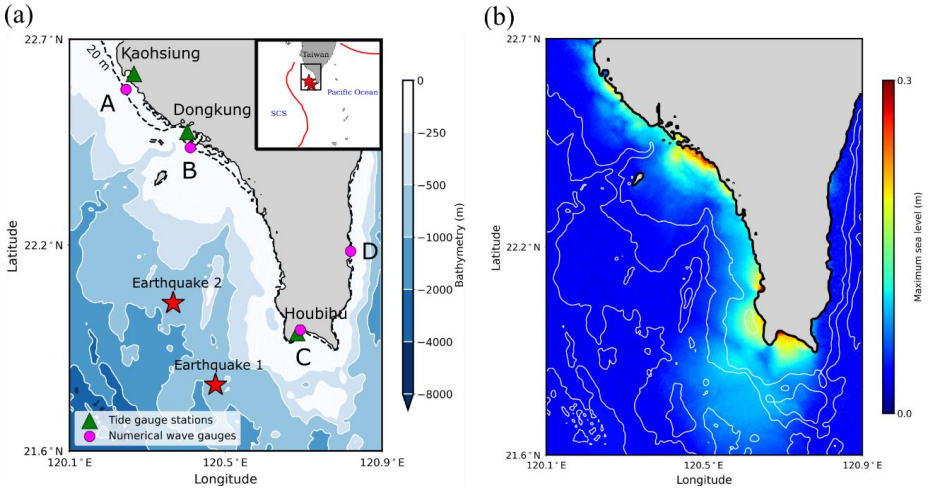

Figure 13. Map of (a) the wide continental shelf in front of Hengchun Peninsula, and (b) the calculated maximum sea level using the GCMT earthquake tsunami scenario. Green triangles indicate the locations of tide gauge stations, and pink circles denote numerical wave gauges. Red stars are the epicenters of the doublet earthquakes. The white solid lines are contour lines, and the black dashed line presents the bathymetric contour at a depth of 20 m.

https://doi.org/10.5194/nhess-2022-126
Preprint. Discussion started: 27 April 2022

Natural Hazards and Earth System Sciences
Discussions

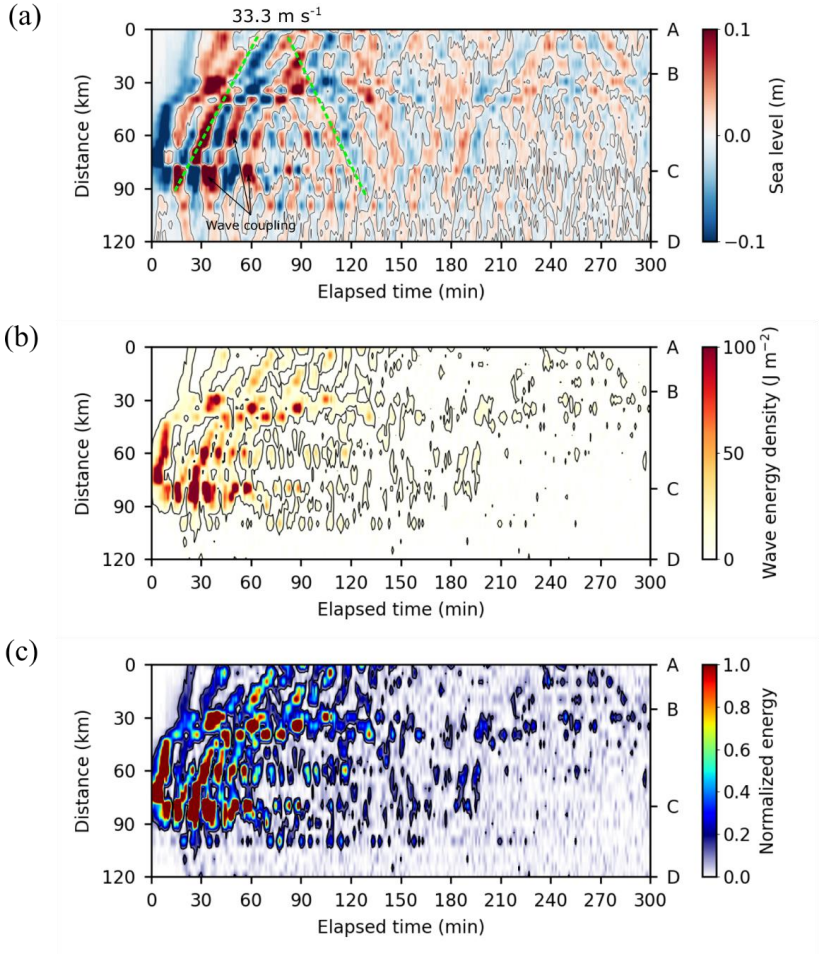

760

Figure 14. Time-distance diagrams of (a) tsunami wave variation, (b) wave energy density, and (c) normalized energy. The green dashed lines illustrate the travel- time curve of edge wave propagation. The black arrows indicate the spatiotemporal locations of wave coupling.